Surface & Coatings Technology 322 (2017) 134–140

Contents lists available at ScienceDirect

Surface & Coatings Technology

journal homepage: www.elsevier.com/locate/surfcoat

Temperature induced superhard CrB_2 coatings with preferred (001) orientation deposited by DC magnetron sputtering technique

Shucan Zhang [a], Zhenyu Wang [a], Peng Guo [a], Peiling Ke [a,*], Magnus Odén [b], Aiying Wang [a,*]

[a] Key Laboratory of Marine Materials and Related Technologies, Zhejiang Key Laboratory of Marine Materials and Protective Technologies, Ningbo Institute of Materials Technology and Engineering, Chinese Academy of Sciences, Ningbo 315201, PR China
[b] Nanostructured Materials, Department of Physics, Chemistry and Biology (IFM), Linköping University, 58183 Linköping, Sweden

ARTICLE INFO

Article history:
Received 20 January 2017
Revised 10 May 2017
Accepted in revised form 11 May 2017
Available online 11 May 2017

Keywords:
CrB_2 coating
DC magnetron sputtering
Microstructure
Superhard

ABSTRACT

The influence of deposition temperature in the range of 100 °C to 400 °C on the microstructure and mechanical properties of CrB_2 coatings by DC magnetron sputtering was studied. The coating texture changed from random mixed orientation with (101) and (001) planes to the preferred (001) orientation when increasing the deposition temperature. Moreover, the microstructure coating evolved from an underdense structure to a bulky columnar structure (~50 nm), and finally to a dense nanoscale columnar structure (~7 nm). This structural densification was mainly attributed to the enhanced atomic surface diffusion with increasing deposition temperature. It resulted in promotion of the (001) preferred orientation and greatly enhanced the mechanical properties. Specifically, when the deposition temperature was 300 °C, the CrB_2 coatings exhibited the highest toughness while superhardness (51 ± 2 GPa) was achieved for coating grown at 400 °C.

1. Introduction

The structure of chromium diboride (CrB_2) exhibits hexagonal symmetry with space group *P*6/mm, in which hexagonal layers of pure chromium and pure boron atoms are alternately stacked along the c-axis [1]. CrB_2 coatings are considered as a strong candidate for wear resistant, anti-corrosion, electrical contact solar and selective absorber applications due to their comprehensively superior properties, such as high melting point (about 2200 °C), high hardness (for bulk about 11–20 GPa), good chemical stability at elevated temperature [2,3], good corrosion-resistant [4], excellent optical properties [5,6] and lower electrical contact resistance [7].

Many efforts have been devoted so far to the effects of the deposition parameters on the microstructure and properties of CrB_2 coatings, such as negative bias voltage, duty factor of sputtering power and inductively coupled plasma (ICP) assisted power [7–10]. These parameters generally determine the kinetic bombardment energies of the ions arriving on the substrate, the plasma density and the ionization of the sputtered species, which thus affect the microstructure and properties of the deposited coating. Choi et al. [10] had reported that, by increasing the ICP assisted power and the negative substrate bias, the preferred orientation of the CrB_2 films was changed from (101) to (001), and the hardness increased from 30 GPa to 54 GPa. In addition to these dynamic parameters, the deposition temperature significantly influences the surface adatom surface mobility and thus affects the structure and properties of coatings [11,12]. However, even though this process parameter is easy to control, no reports exist where its influence has been studied, which includes the influence of deposition temperature on structural evolution and properties of CrB_2 coating is yet to be addressed.

In the present work, CrB_2 coatings were synthesized by a DC magnetron sputtering system with various deposition temperatures. The composition and structural evolution of the CrB_2 coatings were systematically studied. Moreover, the obtained superhard behavior of CrB_2 coating is discussed in terms of the evolution of phase and microstructure.

2. Experimental

CrB_2 coatings were synthesized on single-crystalline Si (100) and cemented carbide (YG8, WC-8 wt% Co) substrates by a direct current magnetron sputtering system using a compound target (392 mm × 92 mm × 4 mm in size) bonded to a copper backing plate. A more detailed description of the deposition system can be found elsewhere [13]. Prior to deposition, the substrates were ultrasonically cleaned in acetone and methanol for 15 min, respectively, and mounted on a sample holder positioned 8 cm from the target surface inside the vacuum chamber. The base pressure of the chamber was kept below 3×10^{-3} Pa. Subsequently, the chamber was backfilled with argon to 0.28 Pa, and the substrates were DC sputter cleaned at a bias of −600 V for 15 min to remove surface contaminations and gain good coating adhesion. During deposition, all the parameters including sputtering power, argon

* Corresponding authors.
E-mail addresses: plke@nimte.ac.cn (P. Ke), aywang@nimte.ac.cn (A. Wang).

http://dx.doi.org/10.1016/j.surfcoat.2017.05.030
0257-8972/

Table 1
Process parameters for CrB_2 coatings deposition.

Parameters	Value
Sputtering power (W)	183
Argon pressure (Pa)	0.28
Target to substrate distance (cm)	8
Deposition time (min)	180
Substrate bias voltage (V)	−100
Deposition temperature (°C)	100, 200, 300, 400

pressure, target-to-substrate distance and deposition time were kept constant, while the deposition temperature was changed. The detailed deposition parameters are summarized in Table 1.

The crystal structures of the coatings deposited on cemented carbide were characterized by X-ray diffractometry (XRD, Bruker D8 Advance diffractometer, Germany), operating in θ-θ configurations and collecting data over a 2θ-range from 20° to 80°. The chemical composition and chemical state of the Cr and B in the coatings were determined by X-ray photoelectron spectroscopy (XPS, Axis ultradld, Japan) using monochromated Al X-ray source at pass energy 160 eV. Before measurement, the sample surface was ion beam etched for 5 min using 2 keV Ar-ions to remove any contaminants. The graphite C 1 s position at 284.6 eV was used as reference for the energy calibration. The microstructure of the coatings deposited on Si (100) wafer was further investigated by high-resolution transmission electron microscopy (TEM, Tecnai F20, US), operated at 200 kV with a point-to-point resolution of 0.24 nm. The TEM samples for cross-sectional view were prepared by grinding, dimpling, and ion-beam milling method. Hardness and Young's modulus were evaluated using a load-controlled MTS NANOG200 nanoindentation equipped with a Berkovich diamond indenter with a tip radius of approximately 150 nm. An optimum load of 12 mN and the indentation depth of approximately 1/10 of the coating thickness were selected to avoid substrate effects and to obtain load independent mechanical properties. For each type of sample, five indents were made on the coatings to evaluate the average hardness (H), Young's modulus (E) from load–displacement curves using the Oliver and Pharr method [14]. Vickers indentation tests were performed on a MVS-1000D1 Automatic digital micro hardness tester with the normal load of 2.94 N.

3. Results and discussion

In order to identify the chemical composition and chemical state of the Cr and B in the coatings deposited at various temperatures, typical high-resolution core-level XPS analyses were carried out, as shown in Fig. 1. The XPS spectra were analyzed by Gaussian fitting, and the graphite C 1s position at 284.6 eV was used as reference for the energy calibration. The Cr 2p spectrum (Fig. 1a) of all coatings presents one spin orbit doublets of Cr 2p1/2 and Cr 2p3/2 with respective binding energies of 574.4 and 583.6 eV, which correspond to CrB_2 [15]. The B 1s peak located at 188.0 eV further supports the existence of CrB_2 [15]. The B/Cr atomic ratio extracted from the XPS data was 2.06, 1.88, 1.90 and 1.94 as the deposition temperature change from 100 to 400 °C, which is close to 2:1. The results show that no significant difference appears in the chemical composition and chemical state of when the deposition temperature is increased from 100 to 400 °C.

Generally, the deposition temperature had great influence on the preferred crystallographic orientation of the coatings [16–18]. Fig. 2 shows the XRD patterns of CrB_2 coatings deposited on cemented carbide at various deposition temperatures. The five peaks marked as WC originated from YG8 substrates. With increasing deposition temperature, the peaks from the coating become more distinct. At the lowest deposition temperature of 100 °C, hexagonal CrB_2 diffraction peaks are just rarely visible, implying a nanocrystalline structure. However, three peaks appeared around 29.1°, 46.0° and 60.2°, respectively corresponding to (001), (101) and (002) plane of hexagonal CrB_2 (PDF34-0369); further increasing the temperature to 300 and 400 °C, the (101) plane disappeared, (001) and (002) plane were enhanced, implying a (001) preferred orientation in the coatings. The grain size calculated by the Debye-Scherrer equation of CrB_2 coatings is 18, 27, 41 and 37 nm for coatings deposited at 100, 200, 300 and 400 °C, respectively.

It has been empirically found that the densely packed basal planes (001) of CrB_2 are low surface energy planes, while polycrystalline coatings with a (101) texture display a relative low strain energy [10,19]. At low deposition temperature, the adatom mobility on the surface of the growing coating is low and the likelihood that they will rearrange to low energy configurations is lower compared to situations with higher mobility. It results in rather imperfect CrB_2 crystals. At high temperatures, atoms gain more thermal energy and consequently vibrate more strongly, migration on the surface is more likely and rearrangements that promotes long range ordering with less defects is enhanced [16], similar to what was reported for WB_2 [18]. Adatom surface diffusion also influences the evolution of coating texture [20–24]. In the case of low surface adatom mobility, adatoms diffuse shorter distances, which increases the probability for formation of high-surface-energy planes. This is consistent with our observations where low deposition temperature resulted in a random distribution of the grains. High deposition temperature results in high surface adatom mobility and longer diffusion distances. In this case, the probability for the adatoms to arrange in low energy configurations is higher and it promotes growth of planes with the lowest surface energy [24]. In this study, the latter situation prevails for the deposition temperatures 300 and 400 °C causing a (001) texture [25].

Fig. 3 shows cross-sectional views of the morphology of CrB_2 coatings deposited at different temperatures. The thickness of CrB_2 coatings deposited at 100, 200, 300 and 400 °C were 0.9, 1.06, 1.27 and 1.19 μm,

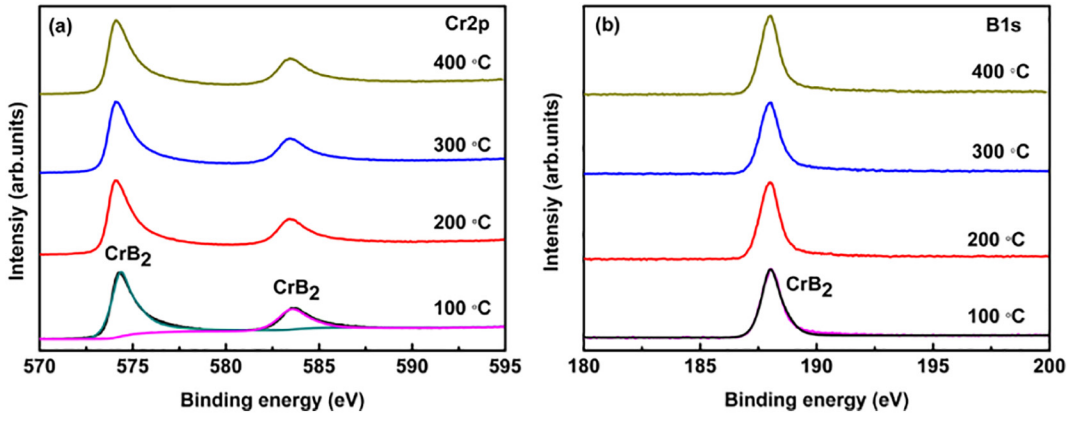

Fig. 1. XPS spectra of CrB_2 coatings with different deposition temperatures.

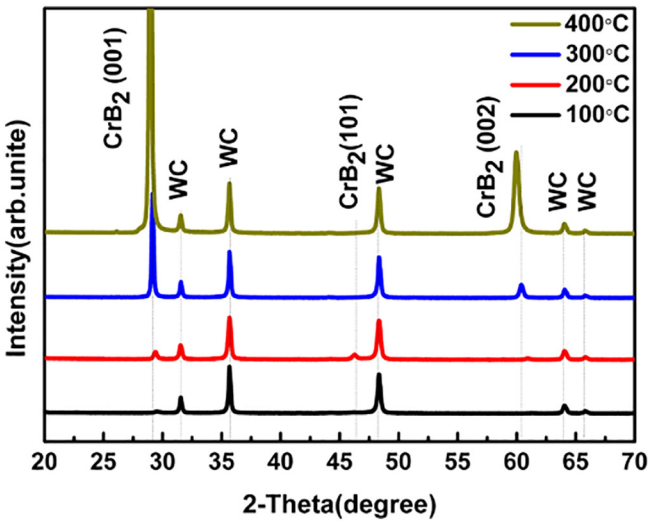

Fig. 2. XRD patterns of CrB_2 coatings with different deposition temperatures.

respectively. The CrB_2 coatings deposited at 100 °C show a fine structure with tendencies for columns in the growth direction (Fig. 3a). At 200, 300 and 400 °C, the coatings exhibit well-developed columnar microstructures, where the columns become more uniform and column boundaries tend to become more narrow with increasing deposited temperature. A contribution to such densification may be attributed to a decreasing amount of voids in the boundaries at high temperature and caused by the higher surface diffusion [26].

High-resolution TEM (HRTEM) and selected area electron diffraction (SAED) were applied to identify the structural evolution with deposition temperatures. Fig. 4 presents cross-sectional TEM micrographs and corresponding SAED patterns of CrB_2 coatings deposited at 100 °C. The SAED pattern shows a broad and diffuse halo, which implies an amorphous or nanocrystalline structure. The TEM images also show the presence of many micro-pores. Using a deposition temperature of 200 °C results in a distinct columnar structure with a columar width of ~50 nm (Fig. 5c). For this sample, the SAED pattern (Fig. 5b) contains three nearly continuous rings corresponding to the (001), (101) and (002) planes of the CrB_2 phase and the HRTEM data (Fig. 5d) clearly show a nanocomposite structure consisting of elongated nanocrystalline grains embedded in an amorphous matrix. The lattice fringe distances in the regions marked as A and B are 1.973 Å and 3.071 Å, which correspond to (101) and (001) planes of CrB_2, respectively. A deposition temperature of 300 and 400 °C leads to ~7 nm wide nanocolumns, as shown in Figs. 6c and 7c. The corresponding SAED patterns of 300 and 400 °C (Figs. 6b and 7b) show four discontinuous rings, which were identified to be (001), (100), (101) and (002) planes of the CrB_2 phase. While, the (100) and (101) peaks did not present in the XRD results, this was probably due to the (100) and (101) peaks were too weak compared with the (001) and (002) peaks. The HRTEM observation of 300 and 400 °C samples (Figs. 6d and 7d) show elongated nanocrystalline grains in an amorphous matrix. The lattice fringes spacing of the crystallization regions was about 3.0710 Å, corresponding to the (001) planes of CrB_2.

Fig. 8 shows the hardness (H), elastic modulus (E) and H/E of the CrB_2 coatings deposited on cemented carbide at various temperatures. As the temperature increased from 100 °C to 400 °C, both of H and E display a monotonous increasing. Specifically, the coating with highest H and E values of 51 ± 2 GPa and 514 ± 10 GPa, respectively, was obtained at 400 °C. Based on the structural analysis and crystallographic orientation evolution, the superhard properties and high elastic modulus could be attributed to the following factors: (1) At this high

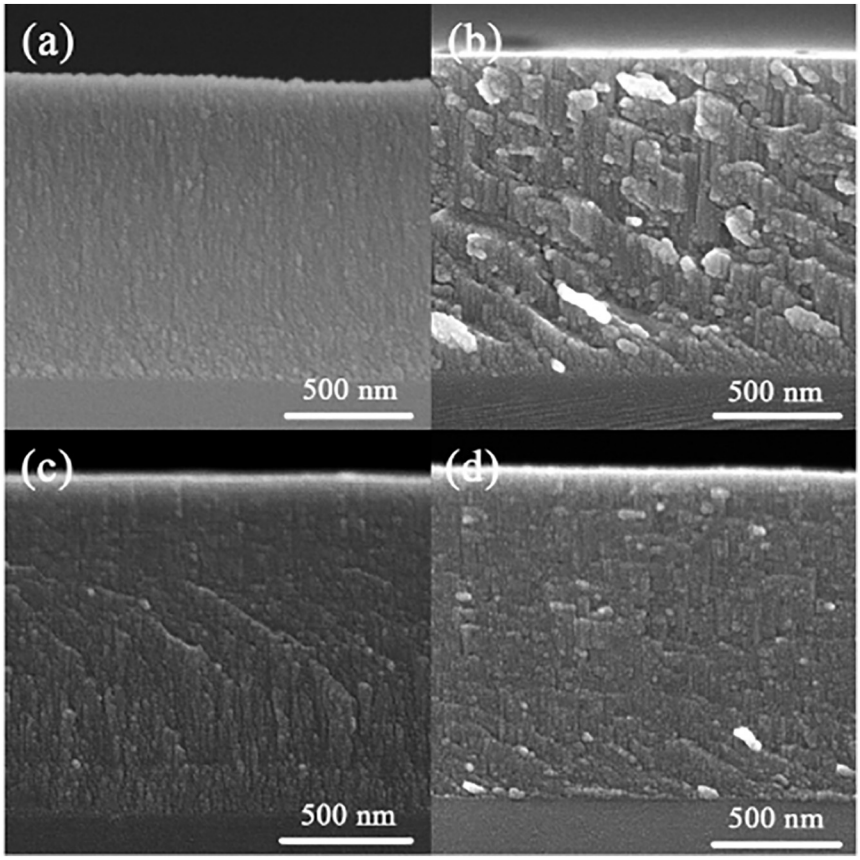

Fig. 3. SEM cross-sectional of CrB_2 coatings with different deposition temperatures: (a) 100 °C, (b) 200 °C, (c) 300 °C and (d) 400 °C.

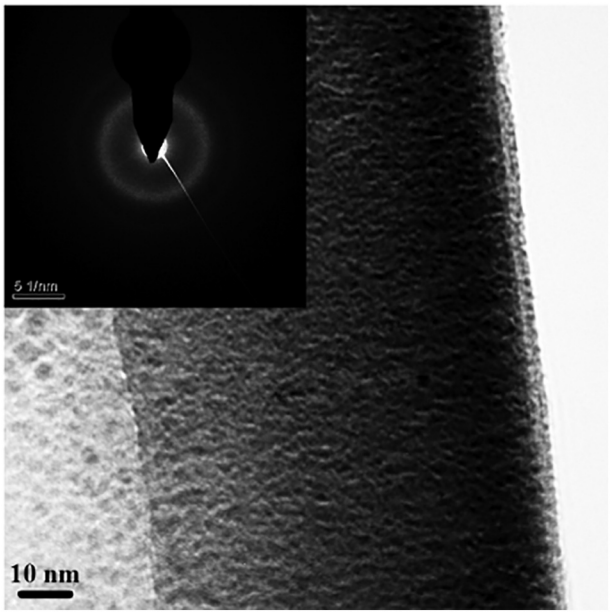

Fig. 4. TEM Cross-sectional images of the CrB_2 coating deposited at 100 °C.

temperature, the adatom mobility was high enough to facilitate a homogenous growth of low energy surfaces in a nanocrystalline manner, and suppress the formation of voids. The fine grain structure effectively restricted formation and glide of dislocations [25]; (2) An elastic anisotropy of the CrB_2 with high elastic stiffness and bonding strength in the ⟨001⟩ direction compared to that in ⟨101⟩ [1,9,10]. In summary, the densely packed nanocolumnar structure with a (001) preferred orientation benefits this CrB_2 coatings superhard properties [27].

Fig. 8(b) shows the H/E ratio of the CrB_2 coatings deposited at various temperatures, which represents fracture toughness. As the deposition temperature increases from 100 °C to 300 °C, the H/E ratio increases from 0.08 to 0.10. Musil et al. [28] has proposed that the coatings exhibit enhanced resistance to cracking when the H/E ratio is beyond 0.1. At 400 °C it decreases slightly by 1.3% as compared with 300 °C. Vickers indentations and corresponding crack patterns (Fig. 9) show a similar trend. The coatings deposited at 100 °C and 200 °C exhibited obvious circular cracks, implying a brittle failure and poor toughness. However, no circular cracks were resolved for the coating deposited at 300 °C, which suggests a relative higher toughness. For the coating deposited at 400 °C, a small amount of circular cracks reformed along the indentation, indicating the decreased toughness.

The change in toughness is closely related to the coatings' microstructure, which in this case are crystalline nanoparticles embedded in an amorphous matrix. The relative amount of amorphous matrix to nanoparticles decreases with increasing deposition temperature. Since energy dissipation during crack growth may occur more or less efficiently depending on the fraction nanoparticles present. For example, shear sliding of the amorphous phase can be suppressed in the presence of nanoparticles resulting in a more brittle behavior and in the opposite manner, nanocrack formation at the interface between the amorphous matrix and nanoscale particles [29,30]. Thus, an optimum of the amount of amorphous matrix is expected and in this case this is achieved for the CrB_2 coatings grown at 300 °C [31].

4. Conclusions

We fabricated CrB_2 coatings by DC magnetron sputtering system using a CrB_2 compound target at different deposition temperatures. It

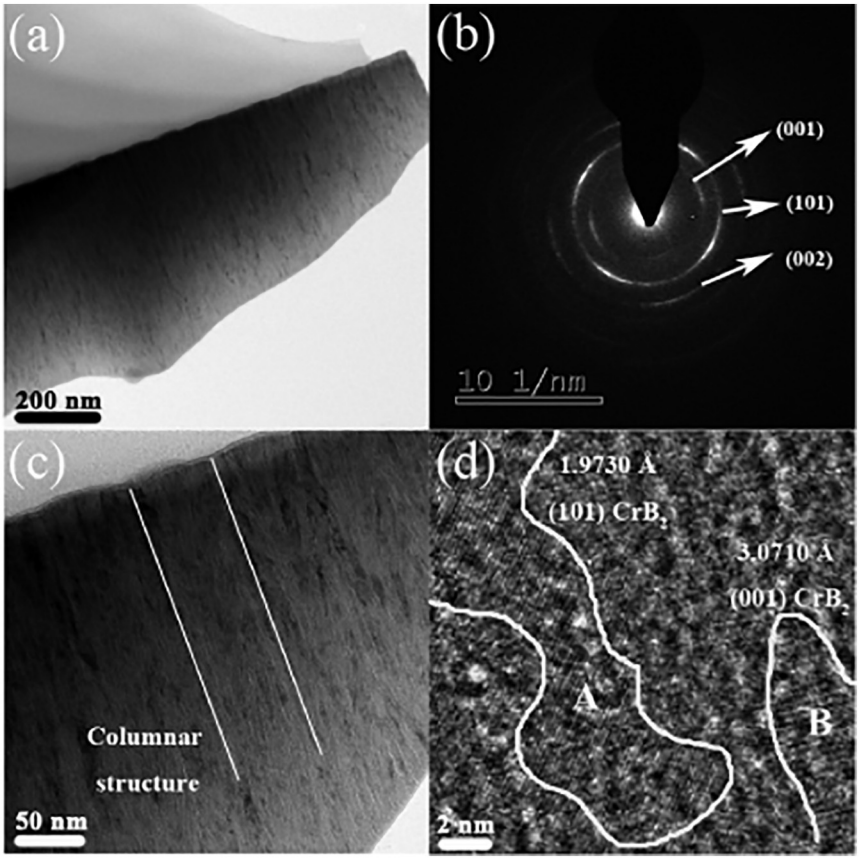

Fig. 5. TEM Cross-sectional images for the CrB_2 coating deposited at 200 °C, region A and B represent the crystalline domain with (101) and (001) plane of CrB_2, respectively.

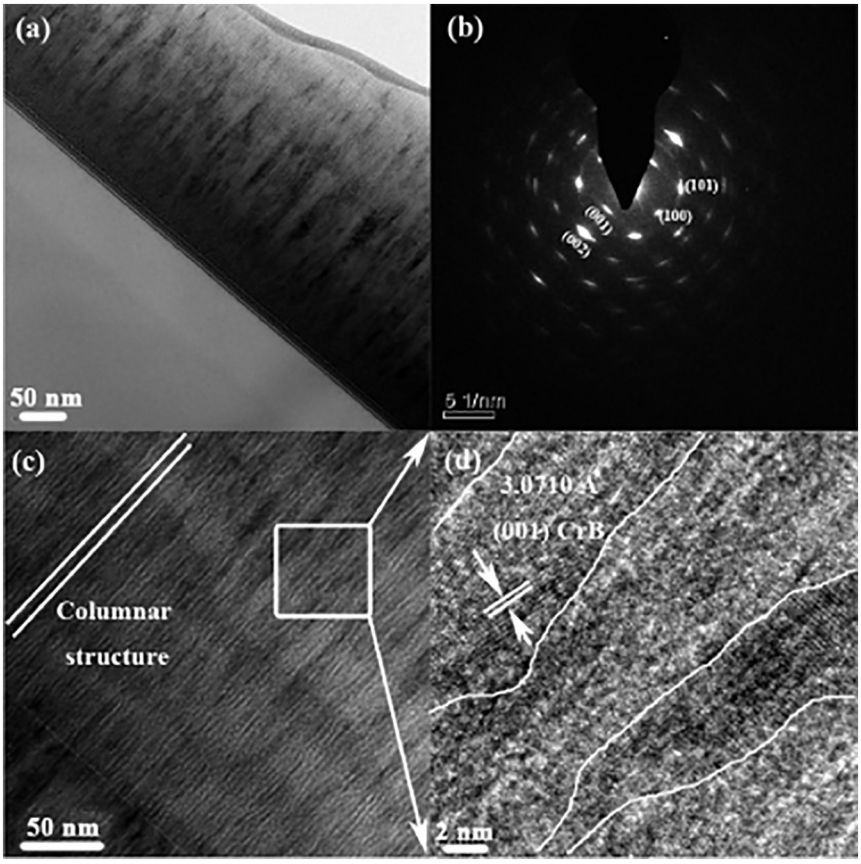

Fig. 6. TEM Cross-sectional images of TEM of the CrB_2 coating deposited at 300 °C.

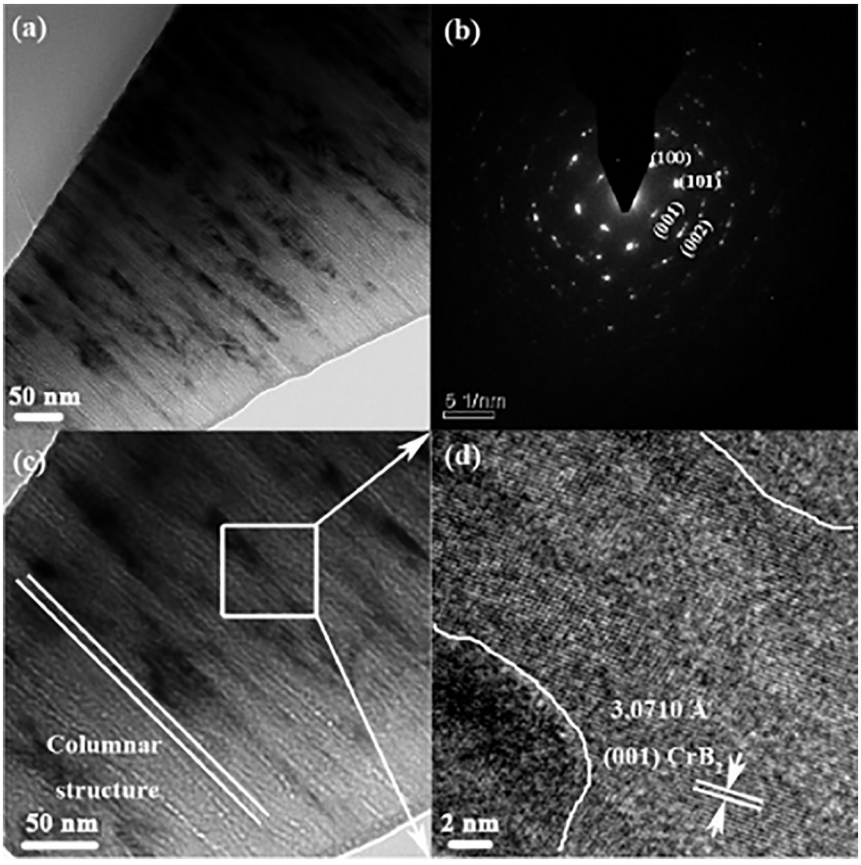

Fig. 7. TEM Cross-sectional images of the CrB_2 coating deposited at 400 °C.

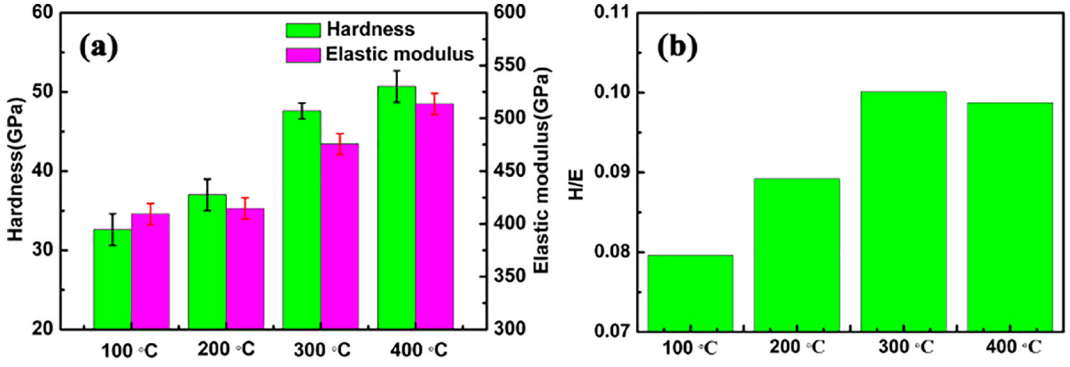

Fig. 8. (a) The hardness (H) and elastic modulus (E) of the CrB_2 coatings deposited at various temperatures; (b) The H/E of the CrB_2 coatings deposited at various temperatures.

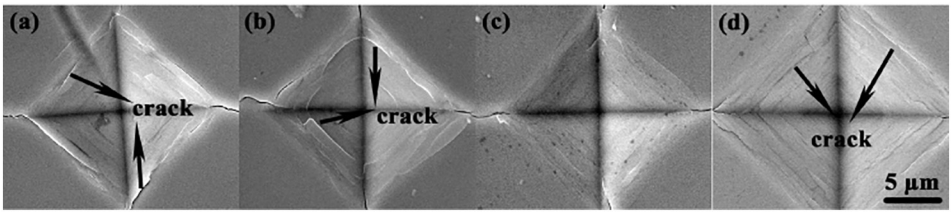

Fig. 9. Vickers indentation morphology of the CrB_2 coatings deposited at various temperatures: (a) 100 °C, (b) 200 °C, (c) 300 °C and (d) 400 °C.

was found that, as the temperature increased from 100 °C to 400 °C, the crystalline texture from random (101) and (001) phase orientation to the (001) preferred one. The morphology changed from glassy to fine columnar due to the increased adatom mobility. The mechanical properties of the CrB_2 coatings were enhanced by this structure evolution and the coatings deposited at 400 °C are superhard with a hardness of 51 ± 2 GPa with fine (001) preferred orientation, which is extremely high for coatings deposited by the traditional DC sputtering technique. In particular, coatings grown at 300 °C exhibited the best toughness.

Acknowledgements

The research was supported by the projects of National Natural Science Foundation of China (51522106, 51611130061), Zhejiang Seagull talent project and Jiangxi Province Science and Technology Project (20161ACE50023). We thank Dr. Xiaowei Li for helpful discussion.

References

[1] N.L. Okamoto, M. Kusakari, K. Tanaka, I. Haruyuki, O. Shigeki, Anisotropic elastic constants and thermal expansivities in monocrystal CrB_2, TiB_2, and ZrB_2, Acta Mater. 58 (1) (2010) 76–84.
[2] A.L. Ivanovskii, Mechanical and electronic properties of diborides of transition 3d-5d, metals from first principles: toward search of novel ultra-incompressible and superhard materials, Prog. Mater. Sci. 57 (2012) 184–228.
[3] X.L. Cui, Y.Y. Wu, T. Gao, X.F. Liu, Influence of preparation temperature on morphology evolution and growth mechanism of CrB_2 in Al–Cr–B alloys, Mater. Lett. 1 (2014) 176–179.
[4] L.R. Jordan, A.J. Betts, K.L. Dahm, P.A. Dearnley, G.A. Wright, Corrosion and passivation mechanism of chromium diboride coatings on stainless steel, Corros. Sci. 47 (2005) 1085–1096.
[5] S. Marka, Menaka, A.K. Ganguli, M.G. Krishna, Effect of substrate and film thickness on the growth, structure, mechanical and optical properties of chromium diboride thin films, Surf. Coat. Technol. 38 (2012) 23–31.
[6] M. Jha, S. Marka, M.G. Krishna, A.K. Ganguli, Multifunctional nanocrystalline chromium boride thin films, Mater. Lett. 73 (2012) 220–222.
[7] N. Nedfors, D. Primetzhofer, L.P. Wang, J. Lu, L. Hultman, U. Jansson, Characterization of magnetron sputtered Cr–B and Cr–B–C thin films for electrical contact applications, Surf. Coat. Technol. 266 (2015) 167–176.
[8] K.L. Dahm, L.R. Jordan, J. Haase, P.A. Deamley, Magnetron sputter deposition of chromium diboride coatings, Surf. Coat. Technol. 108–109 (1998) 413–418.
[9] M. Audronis, P.J. Kelly, R.D. Arnell, A. Leyland, A. Matthews, The structure and properties of chromium diboride coatings deposited by pulsed magnetron sputtering of powder targets, Surf. Coat. Technol. 200 (2005) 1366–1371.
[10] H.S. Choi, B. Park, J.J. Lee, CrB_2 coatings deposited by inductively coupled plasma assisted DC magnetron sputtering, Surf. Coat. Technol. 202 (2007) 982–986.
[11] J.A. Thornton, High rate thick films grows, Annu. Rev. Mater. Res. 7 (4) (2003) 239–260.
[12] P.B. Barna, M. Adamik, Fundamental structure forming phenomena of polycrystalline films and the structure zone models, Thin Solid Films 317 (1998) 27–33.
[13] Z. Wang, J. Liu, L. Wang, X. Li, P. Ke, A. Wang, Dense and high-stability Ti_2AlN MAX phase coatings prepared by the combined cathodic arc/sputter technique, Appl. Surf. Sci. 28 (2017) 1435–1442.
[14] W.C. Oliver, G.M. Pharr, An improved technique for determining hardness and elastic modulus using load and displacement sensing indentation experiments, J. Mater. Res. 7 (1992) 1564–1583.
[15] J.F. Moulder, W.F. Stickle, P.E. Sobol, K.D. Bomben, Handbook of X-ray Photoelectron Spectroscopy, third ed. Physical Electronics, Inc., Eden Prairie, 1995.
[16] A. Vladescu, M. Braic, F.A. Azem, I. Titorencu, V. Braic, V. Pruna, A. Kiss, A.C. Parau, I. Birlik, Effect of the deposition temperature on corrosion resistance and biocompatibility of the hydroxyapatite coatings, Appl. Surf. Sci. 354 (2015) 373–379.
[17] Y.H. Cheng, B.K. Tay, S.P. Lau, Influence of deposition temperature on the structure and internal stress of TiN films deposited by filtered cathodic vacuum arc, J. Vac. Sci. Technol. Technol. A 20 (2002) 1270–1274.
[18] Y.M. Liu, C.L. Jiang, Z.L. Pei, H. Lei, J. Gong, C. Sun, Microstructure and properties of AlB_2-type WB_2 thin films deposited by direct-current magnetron sputtering, Surf. Coat. Technol. 245 (2014) 108–116.
[19] T.F. Zhang, B. Gan, S.M. Park, Q.M. Wang, K.H. Kim, Influence of negative bias voltage and deposition temperature on microstructure and properties of superhard TiB_2 coatings deposited by high power impulse magnetron sputtering, Surf. Coat. Technol. 253 (2014) 115–122.
[20] J.E. Greene, J. Sundgren, L. Hultman, I. Petrov, D.B. Bergstrom, Development of preferred orientation in polycrystalline TiN layers grown by ultrahigh vacuum reactive magnetron sputtering, Appl. Phys. Lett. 67 (1995) 2928–2930.
[21] D. Gall, S. Kodambaka, M.A. Wall, I. Petrov, J.E. Greene, Pathways of atomistic processes on TiN (001) and (111) surfaces during film growth: an ab initio study, J. Appl. Phys. 93 (2003) 9086–9094.
[22] P.H. Mayrhofer, M. Geier, C. Löcker, C. Li, Influence of deposition conditions on texture development and mechanical properties of TiN coatings, Int. J. Mater. Res. 100 (2009) 1052–1058.
[23] S. Matic, Influence of light and temperature on expression of gene Fum1 and on production of fumonisin in three Fusarium species isolated from rice, J. Phys. D. Appl. Phys. 42 (2009) 053002.
[24] Y. Kajikawa, S. Noda, H. Komiyama, Comprehensive perspective on the mechanism of preferred orientation in reactive-sputter-deposited nitrides, J. Vac. Sci. Technol. A 21 (2003) 1943–1954.
[25] P.H. Mayrhofer, C. Mitterer, J.G. Wen, J.E. Greene, I. Petrov, Self-organized nanocolumnar structure in superhard TiB_2 thin films, Appl. Phys. Lett. 86 (2005) 1–3.

[26] Z.H. Xu, Z.K. Wang, J. Niu, L.M. He, R. Mu, K. Wang, Effects of deposition temperature on the kinetics growth and protective properties of aluminide coatings, J. Alloys Compd. 632 (2015) 238–245.
[27] M. Audronis, P.J. Kelly, A. Leyland, A. Matthews, Microstructure of direct current and pulse magnetron sputtered Cr–B coatings, Thin Solid Films 515 (4) (2006) 1511–1516.
[28] J. Musil, Hard nanocomposite coatings: thermal stability, oxidation resistance and toughness, Surf. Coat. Technol. 207 (2012) 50–65.
[29] A. Inoue, X.M. Wang, Bulk amorphous FC20 (Fe–C–Si) alloys with small amounts of B and their crystallized structure and mechanical properties, Acta Mater. 48 (2000) 1383–1395.
[30] J.B. Cheng, X.B. Liang, Z.H. Wang, B.S. Xu, Dry sliding friction and wear properties of metallic glass coating and martensite stainless coating, Tribol. Int. 60 (2013) 140–146.
[31] L.Q. Xing, J. Eckert, L. Schultz, Deformation mechanism of amorphous and partially crystallized alloys, Nanostruct. Mater. 12 (1999) 503–506.